

Instability of an accretion disk with a magnetically driven wind

Xinwu Cao^{1,2}, and H.C. Spruit²

¹ Shanghai Astronomical Observatory, Chinese Academy of Sciences, 80 Nandan Road, Shanghai, 200030, China, and
National Astronomical Observatories, Chinese Academy of Sciences, China

² Max-Planck-Institut für Astrophysik, Postfach 1317, 85741 Garching bei München, Germany

Received ; accepted

Abstract. We present a linear analysis of the stability of accretion disks in which angular momentum is removed by the magnetic torque exerted by a centrifugally driven wind. The effects of the dependence of the wind torque on field strength and inclination, the sub-Keplerian rotation due to magnetic forces, and the compression of the disk by the field are included. A WKB dispersion relation is derived for the stability problem. We find that the disk is always unstable if the wind torque is strong. At lower wind torques instability also occurs provided the rotation is close to Keplerian. The growth time scale of the instability can be as short as the orbital time scale. The instability is mainly the result of the sensitivity of the mass flux to changes in the inclination of the field at the disk surface. Magnetic diffusion in the disk stabilizes if the wind torque is small.

Key words. Accretion, accretion disks–ISM: jets and outflows–*Magnetohydrodynamics*(MHD)

1. Introduction

Magnetically driven winds from accretion disks have been considered as promising explanations for highly collimated jets observed in many classes of astrophysical objects, ranging from active galactic nuclei (AGNs) to young stellar objects (YSOs)(see the reviews by Blandford 1993, 2000; Pringle 1993; Spruit 1996). Hydromagnetic winds from accretion disks provide a mechanism to produce collimated jets as well as an efficient angular momentum loss mechanism from accretion disks. The jets are powered by the gravitational energy released by accretion of matter through a magnetic field with an open configuration. If the inclination angle of the magnetic field lines is sufficient large with respect to the axis of the accretion disk, a magnetically controlled, centrifugally accelerated wind is naturally driven from the disk surface. Open magnetic field lines threading the accretion disks are a crucial ingredient in this model (Blandford & Payne 1982). A global, ordered magnetic field is usually assumed in investigations, though the origin of the ordered magnetic field that is assumed to thread the disk is still not clear. One possibility is that the field is advected inwards by the accreting matter in the disk (Blandford & Payne 1982). The other one is that the field is generated locally by a dynamo (e.g. Tout & Pringle 1996). A steady open magnetic field may be maintained if the inward dragging of field lines by the disk is balanced everywhere by the outward motion of field lines due to magnetic diffusivity (Lubow, Papaloizou, & Pringle 1994a). Lubow, Papaloizou, & Pringle (1994b, here-

after LPP) explored the stability properties of the disk-wind system on the assumption that the angular momentum of accretion disk is removed by the magnetic torque alone. They argue that such a disk wind is unstable. Königl & Wardle (1996) on the other hand claim stability of their own disk-wind solutions (Wardle & Königl 1993). Krasnopolski et al. (1999) also claim stability on the basis of numerical simulations. Instability of the type proposed by LPP has been incorporated into a numerical model by Agapitou and Papaloizou (in preparation).

2. Model

Magnetically driven winds can remove angular momentum from the disk. The wind acceleration is sensitive to the inclination of magnetic field at the disk surface (Blandford & Payne 1982). If the magnetic field is advected inwards by the accreted matter, the field inclination at the disk surface is mainly determined by radial velocity of the matter in the disk. A small perturbation increasing the radial velocity causes the poloidal field to be bent closer to the disk surface, so that it gives rise to a higher mass loss. By the increased angular momentum loss, the radial velocity continues to increase. Thus an instability arises (LPP).

A number of factors have to be included in the analysis. If the magnetic field strength increases inward in the disk, it exerts an outward radial force providing partial support against gravity, so that the rotation of accretion flow is sub-Keplerian. The height of the disk is compressed by both the vertical component of gravitational force and the vertical pressure of the radial magnetic field component.

In principle, one can numerically calculate the disk structure and the magnetic field configuration in the disk simultaneously (Ogilvie 1997, Ogilvie & Livio 1998). For simplicity, in this work we use an approximate field configuration to estimate the scale-height of an isothermal disk compressed by the field.

We assume that the accreting matter is corotating with magnetic field lines in the disk. This is an appropriate limit, if the field is sufficiently strong (e.g. Ogilvie & Livio 2001). The matter at the disk surface is centrifugally accelerated along the magnetic field line anchored at the disk surface. The matter corotates with the magnetic field line roughly till it approaches Alfvén point. Beyond the Alfvén radius, the magnetic field exerts no further torque on the escaping wind matter. The magnetic torque can be estimated if the mass loss rate in the wind and the Alfvén radius are known. As usual, the mass loss rate in the wind is determined by the density at the slow sonic point in the wind. The slow sonic speed is close to the sound speed, if the Alfvén radius $r_A \gg r_s$. To avoid solving the equation of radiative transfer in vertical direction of the disk, we approximate the temperature of the disk to be a constant along the vertical direction.

For most of the stability analysis, a local approximation can be made involving the values of physical quantities near the foot point of a field line. The analysis, however, involves the magnetic torque in an essential way, hence the value of the Alfvén radius r_A for the field line must be known. Since the Alfvén radius depends on the global field configuration, not only on the field strength at the base of the field line, it can be regarded as an external parameter for the stability analysis. To minimize the number of additional parameters in the analysis, we assume the field at the Alfvén surface to be roughly self-similar, varying as a power of distance from the axis. The value of r_A can then be determined and we can evaluate the torque exerted by the wind on the disk. It depends on the mass flux along the field line, which depends on the density at the sonic point. This in turn depends sensitively on both the temperature of the disk and on the inclination and strength of the field near the disk.

Changes in torque exerted cause the mass distribution in the disk to change. This in turn causes changes in the distribution of the field lines anchored in the disk. Since the mass and angular momentum loss rate on a field line depends sensitively on the field configuration (in particular the inclination), there is a strong intrinsic feedback, and it is the purpose of our investigation to see under which conditions this feedback leads to instability of the type proposed by LPP.

The stability problem is in principle global in nature. We localize it by a WKB approximation (short wavelength limit) and a dispersion relation is then derived for the stability problem. This is analogous to the so-called tight-winding approximation used in studies of self-gravitating disks.

A further simplification we make is that the magnetic torque in a steady wind is also be used in the perturbations. This assumption is valid if the time scale of the instability is much longer than the disk-wind coupling time scale. We discuss this further in the last section.

Since our focus is on the instability caused by the wind torque, we leave out angular momentum transported by the

usual disk viscosity, so that viscous modes are also absent in stability analyses. The radial pressure gradient in the momentum equation is neglected for similar reasons, to avoid the presence of an acoustic mode. The circular motion of the disk in equilibrium is given by the balance between the gravity and radial magnetic force. To evaluate the perturbations in the magnetic field above the disk we assume this field to be potential. This a good approximation as long as the Alfvén surface is far from the disk, since the short-wave approximation ensures that the magnetic perturbations decay quickly with height above the disk. The perturbed magnetic field configuration above the disk is then determined by the normal component of the perturbed field at the disk surface. This, in turn, follows from the radial displacements in the disk, through the induction equation. With respect to the magnetic field and the forces it exerts, the model is thus the same as that used earlier by Tagger et al. (1990), Spruit and Taam (1990), Lubow and Spruit (1995), Spruit et al. (1995), and Stehle and Spruit (2001).

To evaluate the mass loss rate in the magnetic wind, a model for the distribution of mass with distance above the mid-plane is needed. We assume the Gaussian distribution valid for an isothermal disk, but also include the effect on the disk thickness of vertical confinement by the magnetic pressures.

Strictly speaking, the presence of a magnetic torque will lead to an azimuthal component of the field. However, the azimuthal field component at the disk surface is always small compared with the radial component for any wind models as long as the Alfvén radius is far from the radius of the field foot-point at the disk mid-plane (see further discussion in section 3.2). If the magnetic field strength inside the disk is sufficiently weak, differential rotation acting on the r - and z -components will produce a time-dependent azimuthal field. Such a nonstationary state will lead to magnetic turbulence such as found in numerical simulations of an initially weak field (Hawley et al. 1995). The field we consider here, on the other hand, is a systematic poloidal field (i.e. crossing the disk plane), and sufficiently strong such that Balbus-Hawley instability is suppressed. At this strength, the field is also sufficiently strong to enforce ‘isorotation’: constancy of the rotation rate along field lines. Though the origin of such fields is not as clear as the turbulent fields that evolve from initially weak seed fields, they are by far the most logical configurations for producing systematic outflows from accretion disks. Spruit et al. (1995), Stehle (1997) and Stehle and Spruit (2001) have shown that even surprisingly strong poloidal fields, approaching (a fraction of) equipartition with orbital kinetic energy, can still be stably anchored in a disk. These analyses did not include instabilities associated with magnetically driven outflows however, which are the subject of the present study.

3. Magnetic torque

From standard magnetic wind theory, we know that the angular momentum flux along a field line is given by $T = \dot{m}\Omega(r_i)r_A^2$, where r is the cylindrical radial coordinate, r_A the Alfvén radius, \dot{m} the mass loss rate, and Ω the rotation rate of the foot-point at radius r_i on the disk. This is the total angular momentum flux, including both the magnetic torque and the flux

carried by the mass itself. For the effect on the disk, only the magnetic torque T_m is consequential; evaluating it at the disk surface, and counting both surfaces, we have

$$T_m = 2\dot{m}\Omega_0(r_i)(r_A^2 - r_i^2), \quad (1)$$

In the limit $r_A \gg r_i$, $T_m \sim 2\dot{m}\Omega_0(r_i)r_A^2$.

The mass loss rate in the wind is governed by the position of the sonic point:

$$\dot{m} \sim \left(\frac{B_z}{B_p}\right) \rho c_s |_{z=z_s}, \quad (2)$$

where z_s is the height of the sonic point above the midplane of the disk.

As discussed in section 2, the mass loss rate of wind from an isothermal disk is estimated as

$$\dot{m} \sim \left(\frac{B_z}{B_p}\right) \rho_0 c_s \exp[-(\Psi_{es} - \Psi_{ei})/c_s^2], \quad (3)$$

where Ψ_{es} and Ψ_{ei} are the effective potential at the sonic point and the footpoint of the magnetic field line respectively. The effective potential Ψ_e is given by

$$\Psi_e(r, z) = -\frac{GM}{(r^2 + z^2)^{1/2}} - \frac{1}{2}\Omega^2(r_i)r^2, \quad (4)$$

where r_i is radius of the magnetic field line footpoint at midplane of the disk.

The position of the sonic point can be estimated, if we know the shape of the magnetic field lines between the footpoint and the sonic point. In principle, the field line shape is computable by solving the radial and vertical momentum equations together with suitable boundary conditions. Analytic solutions are available only for two extreme cases, the weak and strong field extremes. We find that the field line shapes are slightly different in these two extreme cases. In the strong field case, the disk is compressed mainly by the vertical component of magnetic force, and the shape is similar to the Kippenhahn-Schlüter model (KS) (Kippenhahn & Schlüter 1957), valid for an isothermal sheet suspended against gravity by a magnetic field. The exact shape of the field lines depends on the thermal structure of the disk. For our purposes an isothermal layer would be a sufficient model, and the KS model applicable. Its analytic form is still a bit too cumbersome however, so we have approximated it by the following expression:

$$r - r_i = \frac{H}{\kappa_0 \eta_i^2} (1 - \eta_i^2 + \eta_i^2 z^2 H^{-2})^{1/2} - \frac{H}{\kappa_0 \eta_i^2} (1 - \eta_i^2)^{1/2}, \quad (5)$$

where H is the scale height of the disk, $\eta_i = \tanh(1)$. The inclination of the field line $\kappa = B_z/B_r^S$ is a function of z . By the index 0 we denote the value κ_0 measured at the nominal disk surface $z = H$. High above the disk, the inclination then becomes $\kappa_0 \tanh(1)$. We find that this expression reproduces the basic features of the KS model well for both weak and strong field cases.

We approximate the position of the sonic point as the maximum of the effective potential along the magnetic field line.

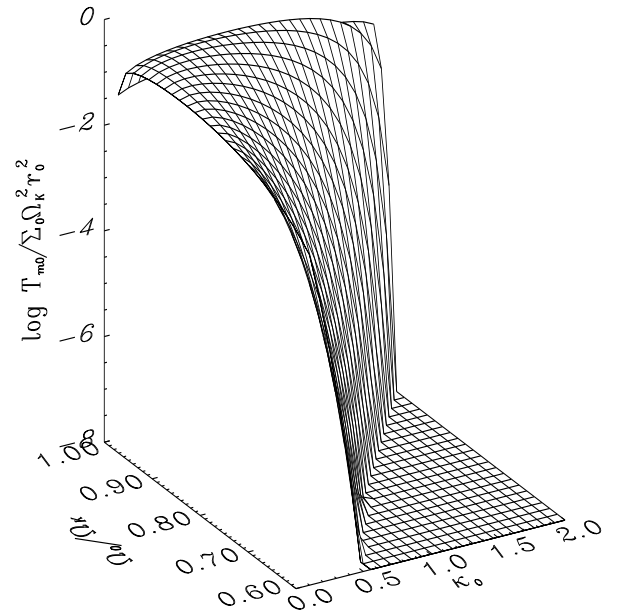


Fig. 1. The magnetic torque as functions of the dimensionless angular velocity of the disk and the magnetic inclination κ_0 , for a disk thickness $H/r = 0.01$. The angular velocity is also a measure of the field strength $(1 - (\Omega_0/\Omega_K)^2 \sim B^2)$.

The height above the disk of the sonic point at radius r_0 of the disk is then from using the potential (4) and the magnetic field line shape (5):

$$z_s \simeq \frac{H}{\eta_i} \left\{ \frac{\kappa_0 \eta_i^2 r_0 (1 - \tilde{\Omega}_0^2) + 3\tilde{\Omega}_0^2 H (1 - \eta_i^2)^{1/2}}{3\tilde{\Omega}_0^2 H - \kappa_0^2 \eta_i^2 H} \right\}^{1/2} - 1 + \eta_i^2, \quad (6)$$

which is valid for $z_s/r_0 \ll 1$.

To complete the estimate, we need the value of the scale height of the disk H , which can be calculated from the vertical component of momentum equation

$$c_s^2 \frac{d\rho(z)}{dz} = -\rho(z) \Omega_K^2 z - \frac{B_r(z)}{4\pi} \frac{dB_r(z)}{dz}. \quad (7)$$

The density distribution $\rho(z)$ in z -direction can be obtained by integrating Eq. (7) with the given field configuration and the assumed disk temperature.

As a result of the magnetic forces the distribution is not exactly the Gaussian distribution of an isothermal disk. The disk thickness is reduced by the magnetic forces. In this case, we define the disk scale height H as $\rho(H) = \rho(0) \exp(-1/2)$, the disk scale height H can then be evaluated numerically. From these numerical values, we have constructed a fitting formula

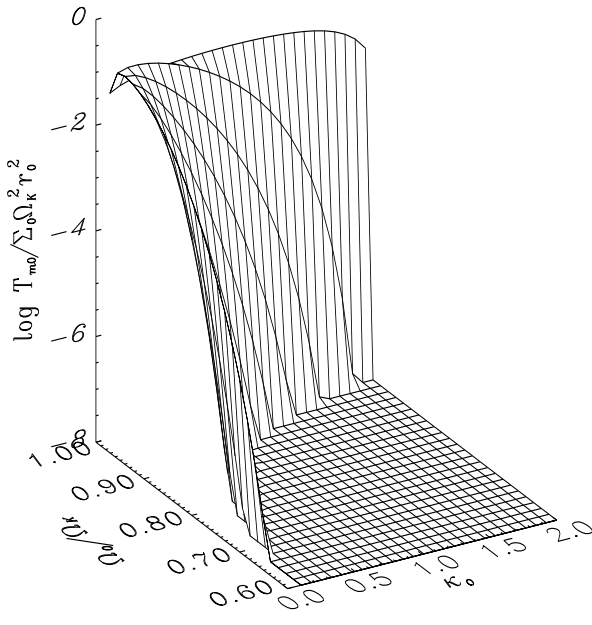


Fig. 2. Same as Fig. 1, but for $H/r = 0.001$.

used in the rest of the calculations to represent the parameter dependence of the scale height H :

$$H = \frac{1}{2} \left[\frac{4c_s^2}{\Omega_K^2} + \frac{(\Omega_K^2 - \Omega_0^2)^2 r_0^2}{4(1 - e^{-1/2})^2 \kappa_0^2 \Omega_K^4} \right]^{1/2} - \frac{(\Omega_K^2 - \Omega_0^2)r_0}{4(1 - e^{-1/2})\kappa_0 \Omega_K^2}. \quad (8)$$

We find that the scale height H given by expression (8) is accurate to about 1% compared with the numerical results in the range of the parameters adopted in this paper. The actual density distribution deviates from a Gaussian distribution, so the density at the sonic point still is only approximate, but the fitting formula properly takes into account the compression of the disk in the strong field case. Note that Eq. (8) reduces to $H = c_s/\Omega_K$ in the Keplerian case. Now, using Eqs. (4)-(6), we obtain the effective potential difference $\Delta\Psi_e$ between the sonic point and the magnetic footpoint in the mid-plane of the disk

$$\Delta\Psi_e = \Psi_{es} - \Psi_{ei} = \frac{1}{2} \Omega_K^2 z_s^2 + \frac{(\Omega_K^2 - \Omega_0^2)r_0 H}{\kappa_0 \eta_i^2} \left[(1 - \eta_i^2 + \eta_i^2 z_s^2 H^{-2})^{1/2} - (1 - \eta_i^2)^{1/2} \right] + \left(\Omega_K^2 - \frac{5}{2} \Omega_0^2 \right) \frac{H^2}{\kappa_0^2 \eta_i^4} \left[(1 - \eta_i^2 + \eta_i^2 z_s^2 H^{-2})^{1/2} - (1 - \eta_i^2)^{1/2} \right]$$

Using Eqs. (3)-(9), we can evaluate the mass loss rate in wind. The magnetic field far from the disk surface is assumed to be roughly self-similar as discussed in section 2:

$$B_p^A \sim B_z(r_0) f \left(\frac{r_A}{r_0} \right) = B_z(r_0) \left(\frac{r_A}{r_0} \right)^{-\alpha}, \quad \alpha > 1, \quad (10)$$

where $B_z(r_0)$ is the z -component of the magnetic field at the disk surface.

At the Alfvén point, the Alfvén velocity is

$$v_A^A = \frac{B_p^A}{(4\pi\rho_A)^{1/2}}, \quad (11)$$

As in all magnetic acceleration models, its value is of the order $v_A^A \sim r_A \Omega_0$, where B_p^A and ρ_A are the poloidal magnetic field strength and density of the outflow at Alfvén point.

Mass and magnetic flux conservation along a magnetic field line requires

$$\frac{\dot{m}}{B_z^d} \sim \frac{\rho_A v_A^A}{B_p^A}. \quad (12)$$

Combining Eqs. (10)-(12), the Alfvén radius is found:

$$r_A \simeq \left[\frac{B_z^d}{4\pi\dot{m}\Omega_0(r_0)} \right]^{\frac{1}{\alpha+1}} r_0^{\frac{\alpha}{\alpha+1}}. \quad (13)$$

Now we can evaluate the magnetic torque T_m by using Eqs (3), (6) and (13).

We define dimensionless quantities by

$$\tilde{T}_m = \frac{T_m}{\Sigma_0 \Omega_K^2 r_0^2}, \quad \tilde{\Omega}_0 = \frac{\Omega_0}{\Omega_K}, \quad \tilde{H} = \frac{H}{r_0}. \quad (14)$$

The dimensionless magnetic torque \tilde{T}_m is then given by

$$\tilde{T}_m = \tilde{\Omega}_0^{\frac{\alpha-1}{\alpha+1}} (1 - \tilde{\Omega}_0^2)^{\frac{2}{\alpha+1}} \kappa_0^{\frac{2}{\alpha+1}} \kappa_s^{\frac{\alpha-1}{\alpha+1}} (1 + \kappa_s^2)^{-\frac{\alpha-1}{2(\alpha+1)}} \left[1 + \frac{1 - \tilde{\Omega}_0^2}{2(1 - e^{-1/2})\kappa_0 \tilde{H}} \right]^{\frac{\alpha-1}{2(\alpha+1)}} \exp \left(-\frac{\alpha-1}{\alpha+1} \frac{\Delta\Psi_e}{c_s^2} \right), \quad (15)$$

The parameters of the model are now \tilde{H} , $\tilde{\Omega}_0$, κ_0 and the self-similarity index α of magnetic field shape. Here κ_s is the inclination of the field line at the sonic point.

3.1. Dependence of the magnetic torque on field strength and inclination

With increasing field strength, the rotation of the disk becomes more sub-Keplerian. Though the increasing field strength itself increases the torque through the increasing Alfvén radius [second factor in Eq. (15)], the lower rotation of the footpoints also increases the potential barrier that the wind has to overcome (last factor). In many cases of interest, an increasing field strength will reduce the magnetic torque (e.g. Shu 1991; Ogilvie & Livio 1998, 2001). In the following, we use the rotation rate relative to Keplerian, $\tilde{\Omega}_0$, as measure of the field strength. Figures 1 and 2 show expression (15) for the cases $\tilde{H} = 0.01$ and $\tilde{H} = 10^{-3}$.

3.2. Azimuthal magnetic field component at the disk surface

The magnetic torque T_m exerted on the unit surface area of the disk is given by

$$T_m = \frac{B_z B_\phi^S r}{2\pi}, \quad (16)$$

where B_ϕ^S is the azimuthal field component at the disk surface. Let g_m be the radial acceleration due to magnetic tension, averaged over the surface mass density of the disk, $g_m = B_r^S B_z / (2\pi\Sigma)$. The radial balance of forces is then $r\Omega_0^2 = g - g_m$. Hence we have the relation

$$\frac{B_\phi^S}{B_r^S} = \frac{\tilde{T}_{m0}}{1 - \tilde{\Omega}_0^2}. \quad (17)$$

For the parameter values where our analysis will be valid, the azimuthal field strength at the disk surface is small, $B_\phi^S \ll B_r^S$ (see Figs. 1 and 2).

4. Disk equations

As discussed in section 2, we neglect the usual disk viscosity in the problem. Torques due to the magnetic wind are therefore the only source of angular momentum loss of the disk material, and in their absence the mass flux through the disk vanishes. The mass conservation and angular momentum equations for the disk are then

$$\left(\frac{\partial}{\partial t} + v_r \frac{\partial}{\partial r} \right) \Sigma + \Sigma \frac{\partial v_r}{\partial r} = 0, \quad (18)$$

and

$$\left(\frac{\partial}{\partial t} + v_r \frac{\partial}{\partial r} \right) v_\phi + \frac{v_r v_\phi}{r} + \frac{T_m}{\Sigma r} = 0, \quad (19)$$

where T_m is the torque contributed by the magnetically driven wind per unit area of disk surface. The radial component of the momentum equation is

$$\left(\frac{\partial}{\partial t} + v_r \frac{\partial}{\partial r} \right) v_r + g - \frac{v_\phi^2}{r} - g_m = 0. \quad (20)$$

where the gravitational and radial magnetic forces are given by $g = GM/r^2$ and $g_m = B_r^S B_z / (2\pi\Sigma)$, and we neglect the gas pressure gradient as discussed in section 2. The magnetic induction equation is

$$\left(\frac{\partial}{\partial t} + v_r \frac{\partial}{\partial r} \right) B_z + \frac{v_r B_z}{r} + B_z \frac{\partial v_r}{\partial r} + \frac{\eta}{r} \frac{\partial}{\partial r} \left(r \frac{\partial B_r}{\partial z} \right) = 0. \quad (21)$$

where η is magnetic diffusivity, H is the disk scale-height.

As discussed in section 2, a potential field above the disk is assumed, so that the stream function of the field satisfies

$$\frac{\partial^2 \Phi}{\partial r^2} - \frac{1}{r} \frac{\partial \Phi}{\partial r} + \frac{\partial^2 \Phi}{\partial z^2} = 0. \quad (22)$$

4.1. Linearized equation in a local approximation

As discussed in section 2, the problem can be localized by a WKB approximation in a short wavelength limit. The perturbed stream function is still given by Eq. (22):

$$\frac{\partial^2 \delta\Phi}{\partial r^2} - \frac{1}{r} \frac{\partial \delta\Phi}{\partial r} + \frac{\partial^2 \delta\Phi}{\partial z^2} = 0. \quad (23)$$

The strength $B_z(r)$ at the disk surface acts as boundary condition for this potential problem. Its solution is in general a global one, the solution at any point (r, z) depends on the entire field strength distribution $B_z(r)$. In a short wavelength limit, however, the problem becomes local again. Our short wavelength limit is the magnetic equivalent of the so-called tight-winding limit in self-gravitating disks.

Equation (23) has separable solutions $\delta\Phi(r, z) = F(r) \exp(-k|z|)$, where $F(r)$ satisfies

$$F'' - \frac{1}{r} F' + k^2 F = 0. \quad (24)$$

Let $y = k(r - r_0)$. In the short-wave limit $kr \gg 1$, we have

$$\frac{d^2 F}{dy^2} - \epsilon \frac{dF}{dy} + F = 0, \quad (25)$$

where $\epsilon = 1/kr$ ($\epsilon \ll 1$).

Denote Eulerian perturbations of a quantity q by δq , Lagrangian perturbations by an index 1 , and the equilibrium state by an index 0 .

The perturbed fraction of the stream function is:

$$\delta\Phi(r, z) = A \exp \left(\frac{\epsilon y}{2} \pm iy - k|z| \right). \quad (26)$$

The perturbed components of the magnetic field are

$$\delta B_r(r, z) = -\frac{1}{r} \frac{\partial \delta\Phi}{\partial z} = \frac{k}{r} \delta\Phi(r, z), \quad (27)$$

and

$$\delta B_z(r, z) = \frac{1}{r} \frac{\partial \delta\Phi}{\partial r} = \frac{1}{r} \left(\frac{\epsilon k}{2} + ik \right) \delta\Phi(r, z). \quad (28)$$

Here we have taken the sign in Eq. (26) to be “+”. The magnetic field components are related by

$$\delta B_z = \delta B_r \left(\frac{\epsilon}{2} + i \right) \approx i \delta B_r. \quad (29)$$

Let a dot be the Lagrangian time derivative, and ξ be the Lagrangian displacement. Neglecting the gradient of r in the background and assuming H to be a constant along r , the linearized equations of the disk are:

$$\Sigma_1 + \Sigma_0 \partial_r \xi_r = 0, \quad (30)$$

$$\ddot{\xi}_\phi + (2\Omega_0 + S)\dot{\xi}_r + \frac{T_{m1}}{\Sigma_0 r} - \frac{T_{m0}}{\Sigma_0^2 r} \Sigma_1 = 0 \quad (31)$$

where the shear rate $S = r(d\Omega_0/dr)$.

$$\ddot{\xi}_r - 2\Omega_0 \dot{\xi}_\phi - g_{m1} = 0, \quad (32)$$

where $r\Omega_0^2 = g - g_m$,

$$\dot{B}_{z1} + B_{z0}\partial_r\dot{\xi}_r + \frac{\eta k}{H}B_{z1} = 0. \quad (33)$$

As discussed in section 2, we assume that the magnetic torque as evaluated for steady conditions are also valid for the perturbations. The magnetic torque T_m is a function of the angular velocity of the flow Ω and the magnetic field inclination κ_0 , $\kappa_0 = B_z/B_r^S$, at the disk surface. The perturbed fraction of the magnetic torque δT_m is given by

$$\begin{aligned} \delta T_m &= \frac{\partial T_m(\kappa, \Omega)}{\partial \kappa} \delta \kappa + \frac{\partial T_m(\kappa, \Omega)}{\partial \Omega} \delta \Omega \\ &= \frac{\partial T_m(\kappa, \Omega)}{\partial \kappa} \left(\frac{\delta B_z}{B_{r0}} + i \frac{B_{z0}\delta B_z}{B_{r0}^2} \right) + \frac{\partial T_m(\kappa, \Omega)}{\partial \Omega} \delta \Omega \\ &= \frac{\partial T_m(\kappa, \Omega)}{\partial \kappa} (\kappa_0 + i\kappa_0^2) \frac{\delta B_z}{B_{z0}} + \frac{\partial T_m(\kappa, \Omega)}{\partial \Omega} \delta \Omega. \end{aligned}$$

where Eq. (29) is used. The perturbed fraction of the radial magnetic force is given by

$$\delta g_m = g_{m0} \left(\frac{\delta B_r}{B_{r0}} + \frac{\delta B_z}{B_{z0}} - \frac{\delta \Sigma}{\Sigma_0} \right). \quad (34)$$

Neglecting the radial gradients of the equilibrium quantities (a local approximation) the Eulerian and Lagrangian variations are equivalent, so that the perturbed torque and magnetic acceleration are

$$T_{m1} = \frac{\partial T_m(\kappa, \Omega)}{\partial \kappa} (\kappa_0 + i\kappa_0^2) \frac{B_{z1}}{B_{z0}} + \frac{\partial T_m(\kappa, \Omega)}{\partial \Omega} \frac{\dot{\xi}_\phi}{r_0} \quad (35)$$

and

$$g_{m1} = g_{m0} \left[(1 - i\kappa_0) \frac{B_{z1}}{B_{z0}} + \partial_r \xi_r \right], \quad (36)$$

where Eq. (30) has been substituted. Combining Eqs. (30)-(33), we have

$$\begin{aligned} \partial_{tt}\ddot{\xi}_r + \left(\frac{1}{\Sigma_0 r^2} \frac{\partial T_m}{\partial \Omega} + \frac{\eta k}{H} \right) \partial_t \ddot{\xi}_r - i\kappa_0 g_{m0} \partial_r \ddot{\xi}_r \\ + \left[2\Omega_0(2\Omega_0 + S) + \frac{\eta k}{\Sigma_0 r^2 H} \frac{\partial T_m}{\partial \Omega} \right] \ddot{\xi}_r \\ - \left[\frac{2\Omega_0}{\Sigma_0 r} \frac{\partial T_m}{\partial \kappa} (\kappa_0 + i\kappa_0^2) - \frac{2\Omega_0 T_{m0}}{\Sigma_0 r} + i \frac{g_{m0}\kappa_0}{\Sigma_0 r^2} \frac{\partial T_m}{\partial \Omega} \right. \\ \left. + \frac{\eta k g_{m0}}{H} \right] \partial_r \dot{\xi}_r + \frac{2\eta k \Omega_0}{H} (2\Omega_0 + S) \dot{\xi}_r \\ - \left(\frac{\eta k g_{m0}}{\Sigma_0 r^2 H} \frac{\partial T_m}{\partial \Omega} - \frac{2\eta k \Omega_0 T_{m0}}{\Sigma_0 r H} \right) \partial_r \xi_r = 0. \end{aligned} \quad (37)$$

5. Dispersion relation

We write the perturbed quantities as

$$\xi_r \sim \exp[i(\omega t + kr)].$$

The dispersion relation follows from Eq. (37):

$$\begin{aligned} \omega^4 - i \left(\frac{1}{\Sigma_0 r^2} \frac{\partial T_m}{\partial \Omega} + \frac{\eta k}{H} \right) \omega^3 \\ - \left[\kappa_0 g_{m0} k + 2\Omega_0(2\Omega_0 + S) + \frac{\eta k}{\Sigma_0 r^2 H} \frac{\partial T_m}{\partial \Omega} \right] \omega^2 \\ + \left[\frac{2k\Omega_0}{\Sigma_0 r} \frac{\partial T_m}{\partial \kappa} (\kappa_0 + i\kappa_0^2) + i \frac{g_{m0}\kappa_0 k}{\Sigma_0 r^2} \frac{\partial T_m}{\partial \Omega} \right. \\ \left. - \frac{2k\Omega_0 T_{m0}}{\Sigma_0 r} + \frac{\eta k^2 g_{m0}}{H} + i \frac{2\eta k \Omega_0}{H} (2\Omega_0 + S) \right] \omega \\ - i \frac{\eta k^2 g_{m0}}{\Sigma_0 r^2 H} \frac{\partial T_m}{\partial \Omega} + i \frac{2\eta k^2 \Omega_0 T_{m0}}{\Sigma_0 r H} = 0. \end{aligned} \quad (38)$$

We use some dimensionless quantities in addition to those defined in Eq. (14):

$$\begin{aligned} \tilde{\lambda} &= \frac{\lambda}{H}, & \tilde{\omega} &= \frac{\omega}{\Omega_K}, & \tilde{S} &= \frac{r_0}{\Omega_K} \frac{d\Omega_0}{dr}, \\ \tilde{g}_{m0} &= \frac{g_{m0}}{r_0 \Omega_K^2}, & \tilde{\eta} &= \frac{\eta}{H^2 \Omega_K}, \end{aligned} \quad (39)$$

and the quantities p, q :

$$\frac{\partial \tilde{T}_m}{\partial \tilde{\Omega}_0} = \frac{p}{\tilde{\Omega}_0} \tilde{T}_{m0}, \quad \frac{\partial \tilde{T}_m}{\partial \kappa} = \frac{q}{\kappa_0} \tilde{T}_{m0},$$

which measure the dependence of the wind torque on the rotation rate and field inclination, respectively.

Equation (38) becomes

$$\begin{aligned} \tilde{\omega}^4 - i \left(\frac{p}{\tilde{\Omega}_0} \tilde{T}_{m0} + \frac{2\pi\tilde{\eta}}{\tilde{\lambda}} \right) \tilde{\omega}^3 - \left[\frac{2\pi\kappa_0}{\tilde{\lambda} \tilde{H}} (1 - \tilde{\Omega}_0^2) \right. \\ \left. + 2\tilde{\Omega}_0(2\tilde{\Omega}_0 + \tilde{S}) + \frac{2\pi p \tilde{\eta} \tilde{T}_{m0}}{\tilde{\Omega}_0} \right] \tilde{\omega}^2 - \left[\frac{4\pi \tilde{\Omega}_0 \tilde{T}_{m0}}{\tilde{\lambda} \tilde{H}} \right. \\ \left. - i \frac{2\pi p \kappa_0 \tilde{T}_{m0}}{\tilde{\lambda} \tilde{\Omega}_0 \tilde{H}} (1 - \tilde{\Omega}_0^2) - \frac{4\pi q \tilde{\Omega}_0}{\tilde{\lambda} \tilde{H}} \tilde{T}_{m0} (1 + i\kappa_0) \right. \\ \left. - \frac{4\pi^2 \tilde{\eta}}{\tilde{\lambda}^2 \tilde{H}} (1 - \tilde{\Omega}_0^2) - i \frac{4\pi \tilde{\eta} \tilde{\Omega}_0}{\tilde{\lambda}} (2\tilde{\Omega}_0 + \tilde{S}) \right] \tilde{\omega} \\ - i \frac{4\pi^2 \tilde{\eta} p \tilde{T}_{m0}}{\tilde{\lambda}^2 \tilde{\Omega}_0 \tilde{H}} (1 - \tilde{\Omega}_0^2) + i \frac{8\pi^2 \tilde{\eta} \tilde{\Omega}_0 \tilde{T}_{m0}}{\tilde{\lambda}^2 \tilde{H}} = 0. \end{aligned} \quad (40)$$

5.1. Restrictions on parameter values

The dispersion relation contains several small parameters, since a number of conditions have to be satisfied for consistency with the assumptions made. For a local approximation to be valid, we must have

$$\lambda/r \ll 1. \quad (41)$$

On the other hand, since we have approximated the disk as thin, the wavelength has to be large compared with the scale height:

$$H \ll \lambda. \quad (42)$$

An unknown in the problem is the magnetic diffusivity, hence we must explore the dependence of the results on η . In our assumptions, we have ignored viscosity in the disk. If the magnetic diffusivity is due to the same small scale process that causes the viscosity, it is then most consistent to set $\eta = 0$ as well. On the other hand, it is instructive to explore the consequences of allowing some diffusion, since it is likely to damp instabilities. With our scalings (39), the relevant value is then $\tilde{\eta} \sim \alpha \sim 1$, where α is the viscosity parameter. We report results for both cases, $\tilde{\eta} \ll 1$ and $\tilde{\eta} \sim 1$.

5.2. Approximate analytic results

The nature of the unstable modes can be explored by looking at limiting cases. We can look at the case where the magnetic torque is weak, $\tilde{T}_{m0} \ll 1$. Assuming $1/\tilde{\lambda}$ and \tilde{T}_{m0} to be the same order and ignoring quadratic and higher terms, the last two terms in Eq. (40) containing $\tilde{T}_{m0}/\tilde{\lambda}$ can be omitted. The dispersion relation reduces to a third-order equation. Let $\tilde{\omega} = \tilde{\omega}_r + i\tilde{\omega}_i$, it can then be separated into two equations:

$$\begin{aligned} \tilde{\omega}_r^3 - & \left[3\tilde{\omega}_i^2 - 2\tilde{\omega}_i \left(\frac{p\tilde{T}_{m0}}{\tilde{\Omega}_0} + \frac{2\pi\tilde{\eta}}{\tilde{\lambda}} \right) + \frac{2\pi p\tilde{\eta}\tilde{T}_{m0}}{\tilde{\Omega}_0} \right. \\ & \left. + 2\tilde{\Omega}_0(2\tilde{\Omega}_0 + \tilde{S}) + \frac{2\pi\kappa_0}{\tilde{\lambda}\tilde{H}}(1 - \tilde{\Omega}_0^2) \right] \tilde{\omega}_r + \frac{4\pi q\tilde{\Omega}_0}{\tilde{\lambda}\tilde{H}}\tilde{T}_{m0} \\ & - \frac{4\pi\tilde{\Omega}_0}{\tilde{\lambda}\tilde{H}}\tilde{T}_{m0} + \frac{4\pi^2\tilde{\eta}}{\tilde{\lambda}^2\tilde{H}}(1 - \tilde{\Omega}_0^2) = 0 \end{aligned} \quad (43)$$

and

$$\begin{aligned} \tilde{\omega}_i^3 - & \left(\frac{p\tilde{T}_{m0}}{\tilde{\Omega}_0} + \frac{2\pi\tilde{\eta}}{\tilde{\lambda}} \right) \tilde{\omega}_i^2 \\ & - \left[3\tilde{\omega}_r^2 - 2\tilde{\Omega}_0(2\tilde{\Omega}_0 + \tilde{S}) - \frac{2\pi\kappa_0}{\tilde{\lambda}\tilde{H}}(1 - \tilde{\Omega}_0^2) - \frac{2\pi p\tilde{\eta}\tilde{T}_{m0}}{\tilde{\Omega}_0} \right] \tilde{\omega}_i \\ & + \left(\frac{p\tilde{T}_{m0}}{\tilde{\Omega}_0} + \frac{2\pi\tilde{\eta}}{\tilde{\lambda}} \right) \tilde{\omega}_r^2 - \frac{4\pi q\kappa_0\tilde{\Omega}_0}{\tilde{\lambda}\tilde{H}}\tilde{T}_{m0} \\ & - \frac{2\pi p\kappa_0}{\tilde{\lambda}\tilde{H}\tilde{\Omega}_0}(1 - \tilde{\Omega}_0^2)\tilde{T}_{m0} - \frac{4\pi\tilde{\eta}\tilde{\Omega}_0}{\tilde{\lambda}}(2\tilde{\Omega}_0 + \tilde{S}) = 0. \end{aligned} \quad (44)$$

5.2.1. $\tilde{\eta} \neq 0, \tilde{T}_{m0} = 0$

We now analyze the marginal stability, i.e., $\tilde{\omega}_i = 0$. In the absence of the magnetic torque ($\tilde{T}_{m0} = 0$), Eqs. (43) and (44) reduce to

$$\begin{aligned} \tilde{\omega}_r^3 - & \left[3\tilde{\omega}_i^2 - \frac{4\pi\tilde{\eta}}{\tilde{\lambda}}\tilde{\omega}_i + 2\tilde{\Omega}_0(2\tilde{\Omega}_0 + \tilde{S}) \right. \\ & \left. + \frac{2\pi\kappa_0}{\tilde{\lambda}\tilde{H}}(1 - \tilde{\Omega}_0^2) \right] \tilde{\omega}_r + \frac{4\pi^2\tilde{\eta}}{\tilde{\lambda}^2\tilde{H}}(1 - \tilde{\Omega}_0^2) = 0 \end{aligned} \quad (45)$$

and

$$\begin{aligned} \tilde{\omega}_i^3 - & \frac{2\pi\tilde{\eta}}{\tilde{\lambda}}\tilde{\omega}_i^2 - \left[3\tilde{\omega}_r^2 - 2\tilde{\Omega}_0(2\tilde{\Omega}_0 + \tilde{S}) \right. \\ & \left. - \frac{2\pi\kappa_0}{\tilde{\lambda}\tilde{H}}(1 - \tilde{\Omega}_0^2) \right] \tilde{\omega}_i + \frac{2\pi\tilde{\eta}}{\tilde{\lambda}}\tilde{\omega}_r^2 - \frac{4\pi\tilde{\eta}\tilde{\Omega}_0}{\tilde{\lambda}}(2\tilde{\Omega}_0 + \tilde{S}) = 0. \end{aligned} \quad (46)$$

Let $\omega_i = 0$ in Eqs. (45) and (46), we have

$$\tilde{\omega}_r = \pm[2\tilde{\Omega}_0(2\tilde{\Omega}_0 + \tilde{S})]^{1/2}, \quad (47)$$

and

$$\tilde{\eta} = \frac{\kappa_0\tilde{\lambda}}{2\pi}\tilde{\omega}_r. \quad (48)$$

Since $\eta > 0$, $\tilde{\omega}_r/\tilde{\lambda}$ has the same sign as κ_0 . Since the field strength will normally (but not necessarily) decrease outward in the disk, the inclination of the field lines will be away from the axis, i.e. $\kappa > 0$. In the absence of diffusion, a transition from stability to instability, if it exists at all, then is possible only for an *inward traveling* wave mode, i.e. $\tilde{\omega}_r/\tilde{\lambda} > 0$.

Further progress can be made if we assume that the diffusivity is small, and by looking at conditions near marginal stability. Treating $\tilde{\eta}$ it as a small quantity of the same order as the other small quantities, i.e.

$$\tilde{\eta} \sim \tilde{\omega}_i \sim 1/\tilde{\lambda},$$

the growth rate is then given by

$$\tilde{\omega}_i \simeq \frac{A_1}{\tilde{\lambda}\tilde{H}(3\tilde{\omega}_r^2 - \omega_0^2)}, \quad (49)$$

where

$$\omega_0^2 = 2\tilde{\Omega}_0(2\tilde{\Omega}_0 + \tilde{S}) + 2\pi\kappa_0(1 - \tilde{\Omega}_0^2)/\tilde{\lambda}\tilde{H}, \quad (50)$$

$$A_1 = 2\pi\tilde{\eta}\tilde{H}\tilde{\omega}_r^2 - 4\pi\tilde{\eta}\tilde{H}\tilde{\Omega}_0(2\tilde{\Omega}_0 + \tilde{S}). \quad (51)$$

The real parts of the roots of the equation are:

$$\tilde{\omega}_{r1} \simeq \frac{C_1}{\tilde{\lambda}^2\tilde{\omega}_0^2\tilde{H}}, \quad (52)$$

where

$$C_1 = 4\pi^2\tilde{\eta}(1 - \tilde{\Omega}_0^2), \quad (53)$$

and

$$\tilde{\omega}_{r2,3} \simeq \pm\tilde{\omega}_0 - \frac{C_1}{2\tilde{\lambda}^2\tilde{H}\tilde{\omega}_0^2}. \quad (54)$$

The imaginary part of $\tilde{\omega}$ for these roots is

$$\tilde{\omega}_{i1} \simeq \frac{4\pi\tilde{\eta}\tilde{\Omega}_0(2\tilde{\Omega}_0 + \tilde{S})}{\tilde{\lambda}\tilde{\omega}_0^2} \quad (55)$$

and

$$\tilde{\omega}_{i2,3} = \frac{\kappa_0 C_1}{2\tilde{\lambda}^2 \tilde{H} \tilde{\omega}_0^2}. \quad (56)$$

The modes 2, 3 have the same growth rate in the limit taken here, where only the first order in $\tilde{\eta}$ is kept. From Eqs. (55) and (56), we find that all three modes are stable in low- $\tilde{\eta}$ limit. It implies that the neutral wave and the outward traveling wave are always stable.

The stability condition for the inward traveling wave mode is

$$\tilde{\eta} < \frac{\kappa_0 \tilde{\lambda}}{2\pi} [2\tilde{\Omega}_0(2\tilde{\Omega}_0 + \tilde{S})]^{1/2}, \quad (57)$$

Since the inclination κ is of order unity, and $\tilde{\eta}, 1/\tilde{\lambda}$ are small numbers, the stability condition is satisfied. Not surprisingly, the disk is stable in the absence of a wind torque.

5.2.2. $\tilde{\eta} = 0, \tilde{T}_{m0} \neq 0$

We now include the magnetic torque. In this section we treat it as a small quantity of same order as the other small quantities in the problem. In the absence of the magnetic diffusion ($\tilde{\eta} = 0$), Eqs. (43) and (44) reduce to

$$\begin{aligned} \tilde{\omega}_r^3 - \left[3\tilde{\omega}_i^2 - \frac{2\tilde{\omega}_i p \tilde{T}_{m0}}{\tilde{\Omega}_0} + 2\tilde{\Omega}_0(2\tilde{\Omega}_0 + \tilde{S}) \right. \\ \left. + \frac{2\pi\kappa_0}{\tilde{\lambda}\tilde{H}}(1 - \tilde{\Omega}_0^2) \right] \tilde{\omega}_r + \frac{4\pi q \tilde{\Omega}_0}{\tilde{\lambda}\tilde{H}} \tilde{T}_{m0} - \frac{4\pi \tilde{\Omega}_0}{\tilde{\lambda}\tilde{H}} \tilde{T}_{m0} = 0 \end{aligned} \quad (58)$$

and

$$\begin{aligned} \tilde{\omega}_i^3 - \frac{p \tilde{T}_{m0}}{\tilde{\Omega}_0} \tilde{\omega}_i^2 - \left[3\tilde{\omega}_r^2 - 2\tilde{\Omega}_0(2\tilde{\Omega}_0 + \tilde{S}) - \frac{2\pi\kappa_0}{\tilde{\lambda}\tilde{H}}(1 - \tilde{\Omega}_0^2) \right] \tilde{\omega}_i \\ + \frac{p \tilde{T}_{m0}}{\tilde{\Omega}_0} \tilde{\omega}_r^2 - \frac{4\pi q \kappa_0 \tilde{\Omega}_0}{\tilde{\lambda}\tilde{H}} \tilde{T}_{m0} - \frac{2\pi p \kappa_0}{\tilde{\lambda}\tilde{H}\tilde{\Omega}_0} (1 - \tilde{\Omega}_0^2) \tilde{T}_{m0} = 0. \end{aligned} \quad (59)$$

We analyze the situation close to marginal stability in the case of low magnetic torque ($\tilde{T}_{m0} \rightarrow 0$). The growth rate is given by

$$\tilde{\omega}_i \simeq \frac{A_2}{\tilde{\lambda}\tilde{H}\tilde{\Omega}_0(3\tilde{\omega}_r^2 - \tilde{\omega}_0^2)}, \quad (60)$$

where

$$A_2 = \tilde{\lambda}\tilde{H}p\tilde{T}_{m0}\tilde{\omega}_r^2 - 4\pi q\kappa_0\tilde{\Omega}_0^2\tilde{T}_{m0} - 2\pi p\kappa_0(1 - \tilde{\Omega}_0^2)\tilde{T}_{m0}. \quad (61)$$

The real parts of the roots of the equation are:

$$\tilde{\omega}_{r1} \simeq \frac{C_2}{\tilde{\lambda}\tilde{H}\tilde{\omega}_0^2}, \quad (62)$$

where

$$C_2 = 4\pi q\tilde{\Omega}_0\tilde{T}_{m0} - 4\pi\tilde{\Omega}_0\tilde{T}_{m0} \quad (63)$$

and

$$\tilde{\omega}_{r2,3} \simeq \pm\tilde{\omega}_0 - \frac{C_2}{2\tilde{\lambda}\tilde{H}\tilde{\omega}_0^2}. \quad (64)$$

The imaginary part of $\tilde{\omega}$ for these roots is

$$\tilde{\omega}_{i1} = [4\pi q\kappa_0\tilde{\Omega}_0^2 + 2\pi p\kappa_0(1 - \tilde{\Omega}_0^2)] \frac{\tilde{T}_{m0}}{\tilde{\lambda}\tilde{H}\tilde{\Omega}_0\tilde{\omega}_0^2} \quad (65)$$

and

$$\tilde{\omega}_{i2,3} = [p\tilde{\lambda}\tilde{H}(2\tilde{\Omega}_0 + \tilde{S}) - 2\pi q\kappa_0\tilde{\Omega}_0] \frac{\tilde{T}_{m0}}{\tilde{\lambda}\tilde{H}\tilde{\omega}_0^2}. \quad (66)$$

The modes 2, 3 have the same growth rate in the limit taken here, where only the first order in $1/\tilde{\lambda}$ and \tilde{T}_{m0} is kept.

5.3. Interpretation of the analytic results

The growth rates of the three modes (65, 66) are all proportional to the magnetic torque. Hence they all qualify as instabilities caused by the coupling between the disk and the outflow, if their ω_i are negative. The first mode, ω_1 is neutral, in the absence of diffusion and magnetic torques. If only magnetic diffusion is included (section 5.2.1), it is a damped mode. Thus, low frequency perturbations are stabilized by magnetic diffusion, in the absence of a magnetic torque. When a magnetic torque is present (section 5.2.2) the sign of the growth rate is determined [see eq (65)] by the quantity $2q\tilde{\Omega}^2 + p(1 - \tilde{\Omega}^2)$. For low field strength, the second term is small, and instability is determined by the sign of q , the rate of change of the magnetic torque with inclination of the field line. As Fig. 1 shows, the magnetic torque increases with decreasing inclination (field lines bent further away from the vertical). This reflects the fact that the centrifugal effect is stronger on field lines that are bent further away from the vertical, increasing the mass flux and magnetic torque. Thus q is negative in the cases of interest, and the growth rate $-\omega_i$ positive. The term involving p , the dependence of the wind torque on rotation rate, is stabilizing since $p > 0$ (cf Fig. 1). In dimensional terms, the approximate condition for instability in the absence of magnetic diffusion and in the limit of a weak magnetic wind torque is thus:

$$\frac{-\partial T_m}{\partial \kappa} > -\frac{g_m}{\kappa} \frac{\partial T_m}{\partial g_m}, \quad (67)$$

where $g_m = (\Omega_K^2 - \Omega^2)r_0 = B_r^S B_z/(2\pi\Sigma)$ is the acceleration due to magnetic support of the disk against gravity. (the minus signs are included because the derivatives are negative in the cases of interest).

This mode evidently represents the sought instability, associated with the dependence of magnetic torque on field line inclination. The result shows, however, that the instability is not governed only by the dependence of the torque on inclination. If the magnetic field is strong enough to change the rotation rate by providing support against gravity, the second term in (65) is important, and its effect stabilizing. This represents the fact that a lower rotation rate increases the height of the potential barrier that the wind has to overcome (cf discussion in

section 3), which decreases the magnetic torque (Ogilvie and Livio, 2001).

We briefly discuss the two oscillatory modes. Since $p > 0$ and $q < 0$ for the cases of interest (Fig.1), eq. eq. (66) shows that these modes are stable. In the limit of $\tilde{\eta} = 0$ and $\tilde{T}_{m0} = 0$, the two modes have the same frequency (cf. Eqs. (54) & (64))

$$\tilde{\omega}_{r2,3} \simeq \pm \left[2\tilde{\Omega}_0(2\tilde{\Omega}_0 + \tilde{S}) + (1 - \tilde{\Omega}_0^2) \frac{2\pi\kappa_0}{\tilde{\lambda}} \right]^{1/2}. \quad (68)$$

$[2\tilde{\Omega}_0(2\tilde{\Omega}_0 + \tilde{S})]^{1/2}$ is the epicyclic frequency associated with the stable angular momentum gradient. The second term represents the restoring force due to the change of inclination of the field lines by the perturbations (note that $1 - \tilde{\Omega}_0^2 \propto B_r B_z$). On its own, this magnetic restoring force would yield a wave with frequency $\omega \propto \lambda^{-1/2}$, like a surface wave. This is the result of the long-range nature of the magnetic perturbations of the potential field outside the disk. These magnetic waves have been analyzed before (Spruit & Taam 1990; Tagger et al. 1990).

6. Numerical Results

We obtain the growth rate of the instabilities by solving Eq. (40) numerically. For the shear rate \tilde{S} we take the Keplerian value $S = -3/2$.

The problem is described by the dimensionless disk scale-height \tilde{H} , the angular velocity of accretion flow $\tilde{\Omega}_0$ which is a measure of the magnetic field strength, the inclination of magnetic field $\kappa_0 = B_z/B_r$ at the disk surface, and the dimensionless magnetic diffusivity $\tilde{\eta}$. The inclination turns out to influence the stability mainly through its effect on the wind torque, which depends sensitively on it (Figs.1, 2). The second main parameter determining the stability is the strength of the magnetic field, which we have expressed throughout this paper by its effect on the rotation rate (relative to the Keplerian rate) and the angular velocity of accretion flow, $\tilde{\Omega}_0 = \Omega/\Omega_K$. With increasing field strength, the magnetic stresses start contributing to the support of the disk against gravity, decreasing the rotation rate.

We take the self-similar index α of the magnetic field shape to be 4 in the following. In Figs. 1 and 2, the magnetic torque as functions of κ_0 and $\tilde{\Omega}_0$ is plotted for different values of the dimensionless disk scale-height \tilde{H} . For small disk scale-height, i.e., if the temperature of gas in the accretion disk is low, the magnetic torque is significant only if the angular velocity is close to Keplerian velocity and the magnetic field inclination angle to the disk surface is low (low κ_0 , see Fig. 2). The numerically determined stability boundaries for the neutral wave mode are plotted in Figs. 3 and 4. It is seen that instability happens in basically two region of parameter space. One is at high wind torque (right side of the diagrams); the instability then happens roughly independent of the strength of the magnetic field. At low wind torques, instability is possible only when the rotation rate is close enough to Keplerian.

Examples of the growth rate of the neutral wave mode for different parameter values are shown in Figures 5-11.

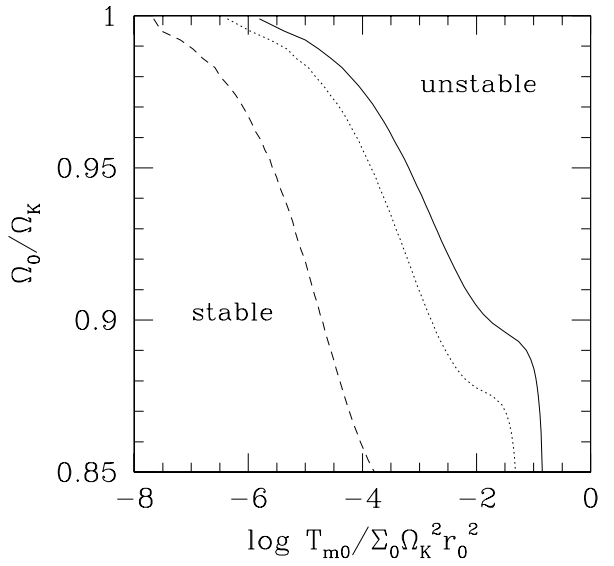


Fig. 3. The stability boundary of the neutral wave mode, for disk thickness $H/r = 0.01$ and wavelength $\lambda/H = 10$, as a function of wind torque and deviation from Kepler rotation. the strength of the magnetic field through the radial equilibrium condition, with high field strength corresponding to low Ω/Ω_K . The dimensionless diffusivity is $\tilde{\eta} = 0.75$ (solid line), 0.25(dotted) and 0.01(dashed).

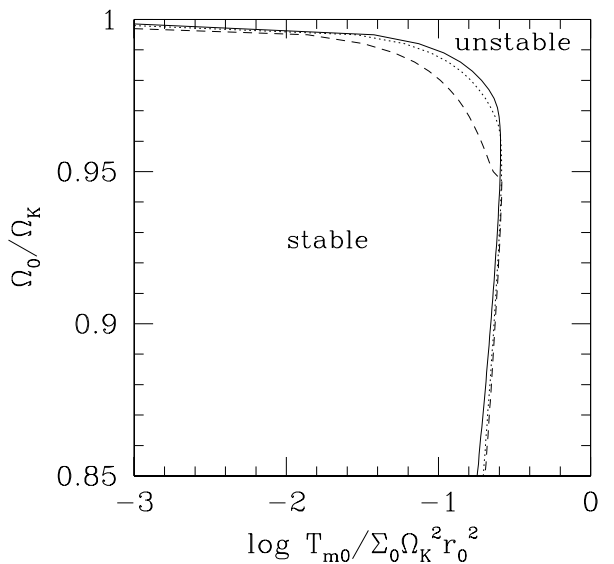


Fig. 4. Same as Fig. 3, but for $H/r = 0.001$.

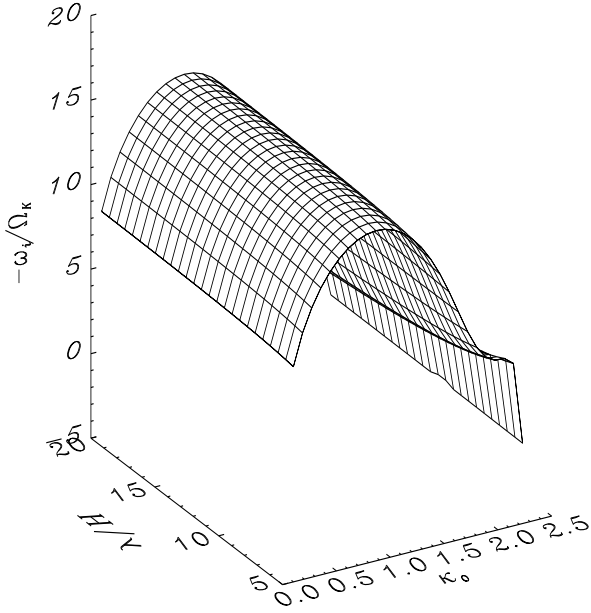


Fig. 5. The growth rate of the instability as functions of magnetic field inclination κ_0 and the dimensionless wavelength λ/H . The dimensionless shearing rate $\tilde{S} = -3/2$, disk thickness $H/r = 0.01$, magnetic diffusivity $\tilde{\eta} = 0.75$ and angular velocity $\Omega_0/\Omega_K = 0.995$ are adopted.

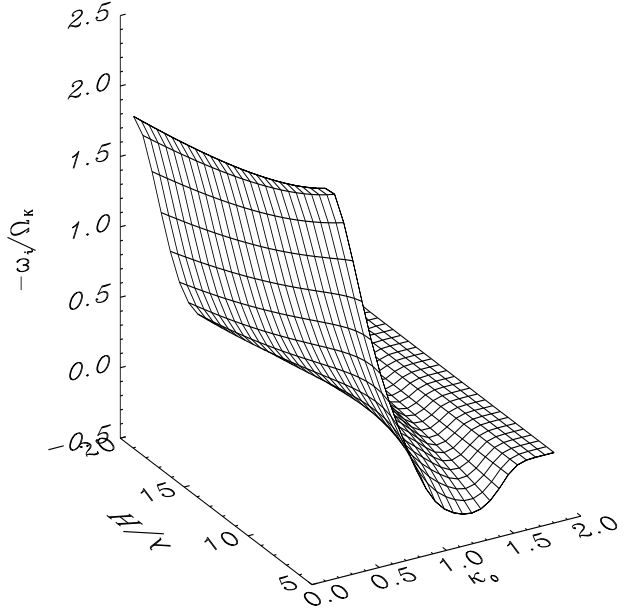


Fig. 7. Same as Fig. 5, but for $\Omega_0/\Omega_K = 0.9$.

7. Discussion of the results

We have presented a linear stability analysis of disks with magnetically driven winds, and confirm the instability by the mechanism proposed by LPP.

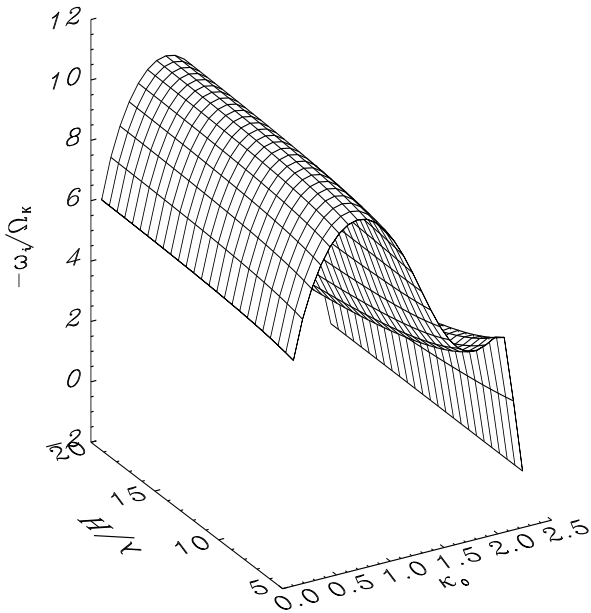


Fig. 6. Same as Fig. 5, but for different value of angular velocity: $\Omega_0/\Omega_K = 0.99$.

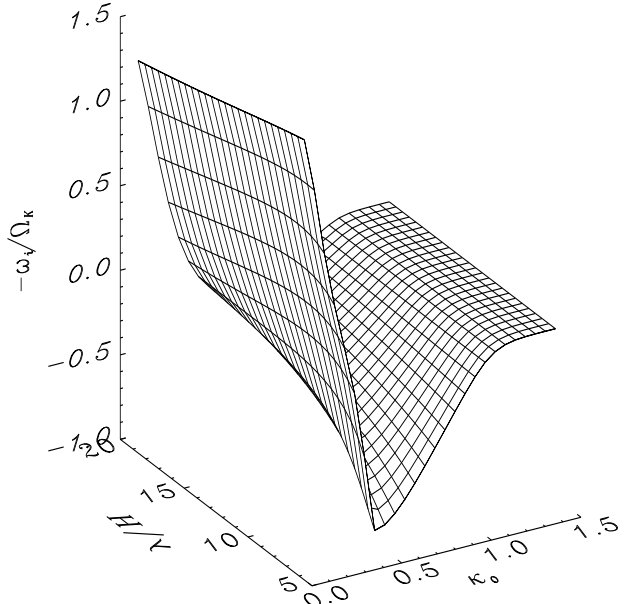


Fig. 8. Same as Fig. 5, but for $\Omega_0/\Omega_K = 0.85$.

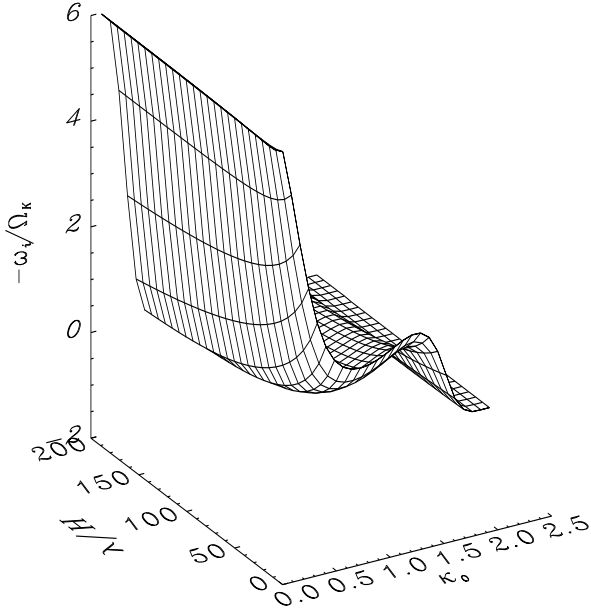


Fig. 9. Same as Fig. 6, but for $H/r = 0.001$.

In the presence of a strong magnetic field, the disk is compressed by the vertical component of gravitational force as well as vertical magnetic pressure, and the vertical structure of the disk is significantly altered, which affects the position of sonic point and the wind torque. In this strong field case, the angular velocity of accretion flow significantly deviates from the Keplerian velocity due to the radial magnetic force, and the magnetic torque is then negligible for any magnetic field inclination angle (see Figs. 1 and 2, see also Ogilvie and Livio 1998). We have taken these effects into account in present investigation.

The system of equations analyzed has four modes. In the absence of a magnetic field, two are a neutral displacements. One of these two is not specifically related to the magnetic wind torque, and we have excluded it from quantitative analysis. The other has a frequency proportional to the magnetic torque (real and imaginary parts of the frequency are of the same order of magnitude), it can become unstable.

The final two modes represent an inward and an outward traveling wave. The restoring force in the wave is a combination of the coriolis force (epicyclic motion) and the magnetic forces. Both inward and outward traveling waves are stable in the range of validity of our assumptions.

In Fig. 5, the growth rate of the instability is plotted for angular velocity very close to Keplerian velocity ($\tilde{\Omega}_0 = 0.995$), which may approximate the case considered in LPP. The disk becomes more unstable if the angular velocity of the flow is close to Keplerian (see Figs. 5-8). For high inclination angles of magnetic field line with respect to the surface of the disk (large κ_0), the magnetic torque is very small. Instability is then suppressed by magnetic diffusion.

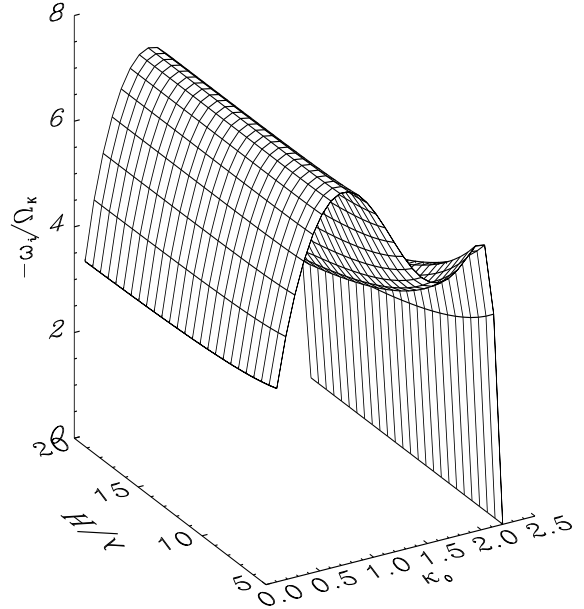


Fig. 10. Same as Fig. 6, but without magnetic diffusion, i.e., $\tilde{\eta} = 0$.

The magnetic torque makes the disk unstable, while magnetic diffusion has a stabilizing effect, suppressing instability at low $\tilde{\Omega}_0$ and/or torque (see Figs. 3 and 4). Comparing Figs. 6 and 9, we see that the disk is less unstable in low temperature case ($\tilde{H} = 0.001$) while the instability occurs for lower values of κ_0 .

To see the effect of magnetic diffusion, Figs. 10 and 11 show the growth rates for the cases with $\tilde{\eta} = 0$. In the absence of magnetic diffusion, the disk is always unstable, though the growth rates can be very small.

The physical reason for the instability found here has been described in LPP (see discussion in section 2). A perturbation increasing v_r causes the poloidal field to be bent close to the disk plane, as the field is advected inwards by the accreting matter. This tends to increase the mass flow along the field. There is also an opposing effect, however. As the poloidal magnetic field is bent towards the disk plane, the radial curvature force on the disk (opposite to gravitational force increases). Due to this increased support against gravity, the rotation rate of the field line decreases. As a result, the “potential barrier” for mass flowing along the field line is larger, decreasing the mass flux and magnetic torque. The instability decreases with increasing field strength through its effect on the rotation rate, since the instability is driven by the magnetic torques. We find that the inclination of the magnetic field still has the strongest influence on the magnetic torque, and dominates over the change in the potential barrier.

Since the instability is caused by the magnetic torque by the centrifugally driven wind from the disk, the instability disappears as the magnetic torque vanishes (Figs. 3 and 4). The

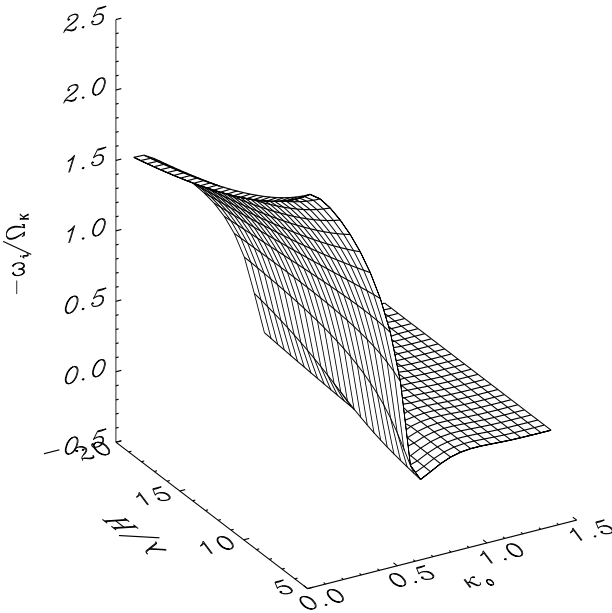


Fig. 11. Same as Fig. 8, but without magnetic diffusion, $\tilde{\eta} = 0$.

disk is stable without a magnetic torque, all three modes are then damped by magnetic diffusion. If the magnetic torque is large, the instability time scale is comparable with the dynamical time scale of the disk, and the instability is not much affected by magnetic diffusion (compare Figs. 6 and 10). We find that the instability is insensitive to the perturbation wavelength.

Associated with the perturbations in the disk are changes of the field configuration above the disk. These affect the acceleration of the wind, and hence the wind torque. In our analysis, we have taken the response of the wind torque to these changes to be instantaneous. This is motivated by the fact that the magnetic torque acts on the disk surface, and changes as soon as the azimuthal field component at the surface changes. This is perhaps somewhat contrary to the impression that one might have based on the steady wind model. In the steady wind model, the torque is often pictured as ‘effectively acting’ at the Alfvén surface. In reality, the torque is constant along the field line, hence acts equally at the disk surface. When changes due to motions in the disk take place, changes in the torque travel up at the Alfvén speed and are first felt in disk itself.

The actual propagation of these torque changes has not been considered here, since its time scale is short, of the order of the Alfvén travel time over the disk thickness. The time scale τ_{Ad} for an Alfvén wave to travel over the scale-height is of the order $\tau_{\text{Ad}} \approx c_s/V_A \Omega^{-1}$, which is short except for weak fields. The time scale for Alfvén wave traveling from the disk surface to the Alfvén point in the wind is in fact shorter than this, $\sim 1/\Omega_0$. The disk-wind coupling time scale is therefore of the order of the disk dynamical time (Wardle & Königl 1993; Königl & Wardle 1996). The present analyses are valid if the instability growth time scale is much longer than the disk-

wind coupling time scale. This is the case since for weak fields, where the coupling time is long, the growth time of the instability itself is also long.

In order to check on the effect of finite Alfvén travel times in the disk-wind coupling process on the instability properties of the disk, we have done a test calculation with a simplified description of this effect. In this calculation, we manually induce a time delay of the dynamical time scale of the disk on the wind torque:

$$\frac{\partial T_m(t)}{\partial t} = \frac{T_{m0} - T_m(t)}{\tau_{\text{delay}}}, \quad (69)$$

where T_{m0} is given by Eq. (15), τ_{delay} is the assumed disk-wind coupling time scale. We then add this equation to the set of disk equations. We find the growth rate of the instability becomes slightly lower than before, but the instability properties have not been altered qualitatively.

The nonlinear evolution of the instability analyzed gas to be studied by numerical simulations. Some such simulations have already been reported by Agapitou & Papaloizou (2001, in preparation).

Acknowledgements. This work was done in the context of the TMR Network ‘accretion onto black holes’ (European Commission grant ERBFMRX-CT98-0195). XC is supported by CAS-MPG exchange program. He thanks the support from NSFC, the NKBRSF (No. G1999075403), and Pandeng Project.

References

- Blandford R.D., 1993, in Burgarella D., Livio M., O’Dea C., eds, *Astrophysical Jets*, Cambridge Univ. Press, Cambridge, p.15
- Blandford R.D., 2000, *Phil. Trans.* 358, 811
- Blandford R.D., Payne D.G., 1982, *MNRAS* 199, 883
- Hawley J.F., Gammie C.F. & Balbus S.A., 1995, *ApJ* 440, 742
- Kippenhahn R., Schlüter A., 1957, *Zeits. Astrophys.* 43, 36
- Königl A., Wardle M., 1996, *MNRAS* 279, L61
- Krasnopoliski R., Li Z. Y., Blandford R., 1999, *ApJ* 526, 631
- Lubow S.H., Papaloizou J.C.B., Pringle J.E., 1994a, *MNRAS* 267, 235
- Lubow S.H., Papaloizou J.C.B., Pringle J.E., 1994b, *MNRAS* 268, 1010 (LPP)
- Lubow S.L. & Spruit H.C., 1995, *ApJ* 445, 337
- Ogilvie G.I., 1997, *MNRAS* 288, 630
- Ogilvie G.I., Livio M., 1998, *ApJ* 499, 329
- Ogilvie G.I., Livio M., 2001, *ApJ* 553, 158
- Pringle J.E., 1993, in Burgarella D., Livio M., O’Dea C., eds, *Astrophysical Jets*, Cambridge Univ. Press, Cambridge, p.1
- Shu F.H., 1991, in Lambert D.L., ed, *Frontiers of stellar evolution*, Astronomical Society of the Pacific Conference Series (ASP), p.23
- Spruit H.C., 1996, in Wijers R.A.M.J., Davis M.B., Tout C.A., eds, *Physical Processes in Binary Stars*, Kluwer Dordrecht, p.249
- Spruit H.C., Taam R.E., 1990, *A&A* 229, 475
- Spruit H.C., Stehle R. & Papaloizou, J.C.B., 1995, *MNRAS* 275, 1223
- Stehle R., 2001 & Spruit H.C, *MNRAS* 323, 587
- Stehle R., 1997, in Spruit H.C. and Meyer-Hofmeister E., *Accretion disks: new aspects*, Lecture Notes in Physics v487, Springer, Heidelberg, p.154
- Tagger M., Henriksen R.N., Sygnet J.F., Pellat R., 1990, *ApJ* 353, 654
- Tout C.A., Pringle J.E., 1996, *MNRAS* 281, 219
- Wardle M., Königl A., 1993, *ApJ* 410, 218